Calculated photoexcitation spectra of positronium Rydberg states

S. D. Hogan
Department of Physics and Astronomy, University College London, Gower Street, London WC1E 6BT, United Kingdom
(Received 22 March 2013; published 25 June 2013)

Calculations of the photoexcitation spectra of ortho-positronium Rydberg states with principal quantum numbers between 10 and 30 are presented. The effects of Doppler broadening and saturation of the corresponding electric-dipole transitions are studied, together with the role of static and motionally induced electric fields. This is done in the context of recent measurements reported by Cassidy *et al.* [Phys. Rev. Lett. **108**, 043401 (2012)], and with regard to experiments involving the production of antihydrogen by charge-exchange between Rydberg positronium and cold antiprotons.

DOI: 10.1103/PhysRevA.87.063423 PACS number(s): 32.80.Rm, 36.10.Dr, 32.60.+i

I. INTRODUCTION

Recent developments in the efficient production of dense, low-energy samples of ortho-positronium (ortho-Ps) [1–3], and the subsequent photoexcitation of these samples to Rydberg states of high principal quantum number n [4], have opened up exciting opportunities for studies involving these exotic atoms. These opportunities lie in the areas of (i) precision spectroscopic measurements associated with the accurate determination of the Rydberg constant, which may shed light on the proton size anomaly [5,6], (ii) the implementation of efficient methods for the production of antihydrogen by charge-exchange [7–9], and (iii) studies of the interaction of particles composed of antimatter with the gravitational field of the Earth [10]. In each of these areas it is foreseen to exploit the large electric-dipole moments associated with the Ps Rydberg states to implement Rydberg atom optics elements including mirrors [11], lenses [12], and traps [13–15] as have been demonstrated for other atoms and molecules.

Following the early work of Chu, Mills, and coworkers on the measurement of the $1S$-$2S$ transition frequency in ortho-Ps [16–18], the resonant two-photon excitation of Rydberg states, with principal quantum numbers up to $n \simeq 19$, was first reported by Ziock *et al.* [19]. More recently, the efficient photoexcitation of Rydberg states of ortho-Ps with values of n as high as 25, by Cassidy *et al.* [4], has made the preparation of selected Rydberg-Stark states, with precisely defined electric-dipole moments, a realistic prospect.

In this article, calculated photoexcitation spectra of Rydberg states of ortho-Ps are presented. The effects of Doppler broadening and saturation of the corresponding electric-dipole transitions are determined together with the role of electric and magnetic fields in the photoexcitation volume. This treatment is carried out in the context of the recent experiments of Cassidy *et al.* [4], and that of the AE$\bar{\text{g}}$IS antihydrogen experiment [9] currently under construction at CERN. In the AE$\bar{\text{g}}$IS experiment, the efficient preparation of Rydberg Ps will be essential to achieve controlled production of antihydrogen by charge-exchange between these excited atoms and cold trapped antiprotons. The results of the calculations presented here allow a qualitative characterization of the magnitude of the electric fields present in the experiments of Cassidy *et al.* [4], and permit identification of the experimental requirements for the efficient photoexcitation of selected Rydberg-Stark states of ortho-Ps. The preparation of such states is of particular importance for the efficient implementation of Rydberg atom optics elements. It is also crucial for the controlled transfer of population from the low-$|m|$ Rydberg states, where m is the azimuthal quantum number, accessible by laser photoexcitation from the ground state, to the longer-lived high-$|m|$ states [20,21], which will be of importance for gravity measurements using Ps [10].

II. RYDBERG STATES OF POSITRONIUM

All electronic states of Ps, including the ground state, exhibit finite lifetimes. The decay rate of the $1s$ ground state is governed solely by the electron-positron annihilation rate, while annihilation and spontaneous emission contribute to the rate of decay of the excited states. These two quantities both depend strongly upon the value of the principal quantum number n.

For exotic atoms such as Ps, which are unstable toward annihilation, the annihilation rates of excited electronic states, $|n\ell\rangle$, with orbital angular momentum quantum number ℓ, depend upon the probability density, and hence the square of the excited state wave function, evaluated at $r = 0$ (the origin of the spherical polar coordinate system). As a result, the Ps annihilation rate for each series of Rydberg states with a particular value of ℓ, scales with n^{-3} (i.e., the annihilation lifetime scales with n^3) [22]. This reduction in annihilation rate as n increases makes the preparation of high-n Rydberg states of particular interest in the areas of research outlined above.

The $1s$ ground electronic state of Ps is composed of two spin states: a singlet state (para-Ps) and a triplet state (ortho-Ps), with lifetimes of 125 ps [23] and 142 ns [24], respectively. The longer lifetime of ortho-Ps makes it most suitable for experiments involving pulsed laser photoexcitation as these are generally performed with laser pulses of $\sim$10 ns duration. In the $2s$ state of ortho-Ps, the strong dependence of the annihilation rate on the value of n leads to an annihilation lifetime of approximately 1 μs.

However, in the $2p$ state, since the centrifugal barrier further reduces the spatial overlap of the electron and positron wave functions at short range, the annihilation lifetime exceeds 100 μs [25,26].

In the absence of external fields, the spontaneous emission rates of atomic Rydberg states with low values of ℓ also scale with n^{-3} (i.e., $\tau_{\rm fluor} \propto n^3$) [27]. The field-free fluorescence lifetime, which in the case of the $2p$ state is equal to the inverse of the Einstein-A coefficient, $A_{1s,2p}$, for the transition to the $1s$ state, is

$$\tau_{\rm fluor}(2p) = A^{-1}_{1s,2p} = \left[\frac{2e^2\omega^3_{1s,2p}}{3\epsilon_0 hc^3}\frac{1}{3}|\langle 1s|r|2p\rangle|^2\right]^{-1}, \\ = 3.19\text{ns} \quad (1)$$

where e, ϵ_0, h, and c are the electron charge, the vacuum permittivity, Planck's constant, and the speed of light in vacuum, respectively; $\omega_{1s,2p} = 2\pi\, c\,(\frac{1}{1^2} - \frac{1}{2^2})\,{\rm Ry}_{\rm Ps}$ is the angular frequency corresponding to the energy difference between the $1s$ and $2p$ states, with the Rydberg constant for Ps, ${\rm Ry}_{\rm Ps} = \frac{1}{2}{\rm Ry}_\infty$, where ${\rm Ry}_\infty$ is the Rydberg constant for a system with an infinitely heavy ion core; and $\langle 1s|r|2p\rangle = 1.29\, a_{0_{\rm Ps}}$ is the radial integral associated with the overlap of the $1s$ and $2p$ wave functions, such that the Bohr radius for Ps, $a_{0_{\rm Ps}} = 2\, a_0$, where a_0 is the Bohr radius of a system with an infinitely heavy ion core. Because of the effects of the reduced mass on the Rydberg constant and on the Bohr radius, the fluorescence lifetime of the $2p$ state in Ps is 1.999 times that in the hydrogen atom. In general the lifetimes of the excited electronic states of ortho-Ps are longer than those of the corresponding states in atomic hydrogen and their rate of decay is dominated by fluorescence rather than annihilation. Rydberg states of Ps are therefore ideally suited to deceleration and electrostatic trapping using inhomogeneous electric fields as has been achieved for atomic hydrogen [13–15].

III. PHOTOEXCITATION OF FIELD-FREE RYDBERG STATES

In the work of Ziock *et al.* [19] and that of Cassidy *et al.* [4], Rydberg states of ortho-Ps were excited using a resonant $1s \rightarrow 2p \rightarrow ns/nd$ two-photon excitation scheme. This scheme requires the generation of laser light at 41 151.493 cm^{-1} (corresponding to a vacuum wavelength, $\lambda_{\rm vac} = 243.004$ nm) for the $1s \rightarrow 2p$ transition, and between 13 168.478 cm^{-1} ($\lambda_{\rm vac} = 759.389$ nm) and 13 717.164 cm^{-1} ($\lambda_{\rm vac} = 729.014$ nm) for transitions from the $2p$ state to field-free Rydberg states between $n = 10$ and the ionization limit, respectively. At present it is planned to implement a similar two-photon excitation scheme, but via the $3p$ state, for the photoexcitation of Rydberg states of ortho-Ps in the AEgIS antihydrogen experiment [28]. The choice of the $3p$ state as the intermediate state slightly reduces the laser intensity required to saturate the transition to the Rydberg states. While the details of the following discussion are based upon the $1s \rightarrow 2p \rightarrow ns/nd$ photoexcitation scheme, as it is the one for which the experimental data exists, the results are also directly relevant to photoexcitation via the $3p$ state since all of the important features of the calculated photoexcitation spectra are associated with the properties of the Rydberg states and not the intermediate state.

As a consequence of the sensitivity of high Rydberg states to electric, magnetic, and blackbody-radiation fields, the selective photoexcitation of individual quantum states, in this case individual Rydberg-Stark states, is in general governed by the interaction of the Rydberg states with their environment and hence the last step in a resonant multiphoton excitation scheme. In the absence of external fields the spectral intensity $S_{n\ell,2p}$, of an electric-dipole transition from the $2p$ state in Ps to an $|n\ell\rangle$ Rydberg state is proportional to the square of the transition moment, $\langle n\ell|\mu|2p\rangle$, where $\mu = -e\mathbf{r}$. The transition moment can be expressed as the product of a radial integral $D_{n\ell,2p} = \langle n\ell|r|2p\rangle$, and an angular integral $\mathcal{I}$, such that $S_{n\ell,2p} = e^2\,|\mathcal{I}\,D_{n\ell,2p}|^2$.

The values of m, and hence ℓ, of the excited Rydberg states are dependent upon the choice of polarization of the laser radiation employed for each step in the photoexcitation process. The integrals $D^2_{ns,2p} = |\langle ns|r|2p\rangle|^2$ and $D^2_{nd,2p} = |\langle nd|r|2p\rangle|^2$, which are proportional to the spectral intensity, can be calculated using hydrogenic wave functions [29] with the Bohr radius corrected for the reduced mass of Ps. The values of these integrals, for transitions to Rydberg states with values of n between 10 and 50, are presented in Fig. 1. Corresponding numerical data is provided in the Appendix in Table II. From this data, the origin of the strong n dependence of the spectral intensity of Rydberg photoexcitation spectra can be clearly seen. It is also noticeable that the squares of the integrals associated with the $2p \rightarrow nd$ transitions are approximately 16 times greater than those associated with the $2p \rightarrow ns$ transitions.

For each allowed electric-dipole transition from the $2p$ state to the ns Rydberg states (i.e., for $\Delta m = 0$ or ± 1) the square of the angular integral, $\mathcal{I}^2 = 1/3$, as determined using standard angular momentum algebra [29]. For the transitions from the $2p$ state to the nd Rydberg states the numerical values of $\mathcal{I}^2$ are displayed in Table I. It can be seen from this data that the

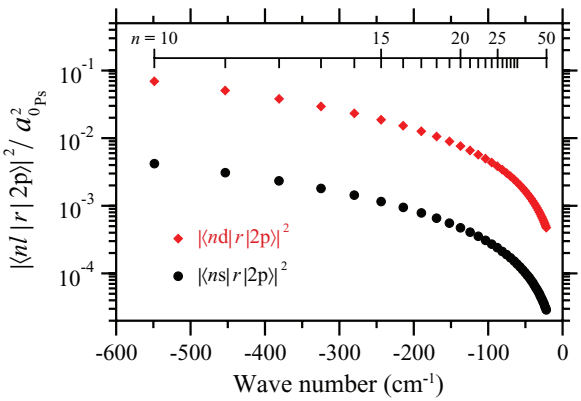

FIG. 1. (Color online) Radial integrals associated with transitions between the $2p$ state, and ns (black circles) and nd (red diamonds) states of Ps. The wave number on the horizontal axis is displayed with respect to the ionization limit.

TABLE I. Numerical values of $\mathcal{I}^2$, the square of the angular integral, associated with the spectral intensity of the $2p \rightarrow nd$ transitions in Ps. The azimuthal quantum numbers associated with the $2p$ state are labeled m while those of the nd Rydberg states are labeled m'.

$\mathcal{I}^2$	$m=-1$	$m=0$	$m=+1$
$m'=-2$	2/5	0	0
$m'=-1$	1/5	1/5	0
$m'=0$	1/15	4/15	1/15
$m'=+1$	0	1/5	1/5
$m'=+2$	0	0	2/5

angular component of the spectral intensity of the $2p \rightarrow nd$ transition is dependent upon the azimuthal quantum number m of the $2p$ state, and the value of Δm. The strongest transitions are those for which $m = \pm 1$ and $\Delta m = \pm 1$, while the weakest are those for which $m = \pm 1$ and $\Delta m = \mp 1$.

These two observations, regarding the ℓ dependence of the radial integrals and the ℓ and m dependence of the angular integrals, indicate that the strongest transitions in the $1s \rightarrow 2p \rightarrow ns/nd$ resonant two-photon excitation scheme under consideration are those from the $|m| = 1$ components of the $2p$ state to the $|m| = 2$ components of the nd Rydberg states. These transitions can be most effectively driven by two circularly polarized laser beams. However, they will also be the dominant transitions observed if photoexcitation is performed with arbitrarily polarized laser beams or in the presence of a randomly oriented electric field.

The spectral intensities of the allowed electric-dipole transitions for each value of Δm can be seen in Fig. 2. Figure 2(a) represents the case for the $2p \rightarrow ns$ transitions, while each of the cases associated with the $2p \rightarrow nd$ transitions are displayed in Figs. 2(b)–2(e). These panels are labeled according to the value of $\mathcal{I}^2$ so that the corresponding values of m and m' can be identified in Table I. The n dependence and relative intensities of each spectral component can be clearly seen in these calculated spectra.

For the strongest set of allowed electric-dipole transitions from the $2p$ state to the nd Rydberg series with $|m| = 2$, a calculated spectrum, corresponding to photoexcitation from the $2p$ state with $m = +1$ using Fourier-transform-limited, single-mode, pulsed laser radiation with a bandwidth of 2.8 cm^{-1} (85 GHz, a bandwidth of approximately that employed by Cassidy *et al.* [4]), can be determined by convolution of the data in Fig. 2(e) with the appropriate Gaussian spectral profile. The result of this can be seen in Fig. 3(a) (continuous blue curve). Under these conditions the strong n dependence of the spectral intensity remains until approximately $n = 30$ where the laser bandwidth is not sufficient to resolve the individual Rydberg states and the spectrum becomes a continuum.

The small mass of Ps means that even at comparatively low translational temperatures motional effects can contribute significantly to the photoexcitation spectra. Under the experimental conditions of Cassidy *et al.* [4], which are not dissimilar to those expected in the AEgIS experiment, the mean Ps

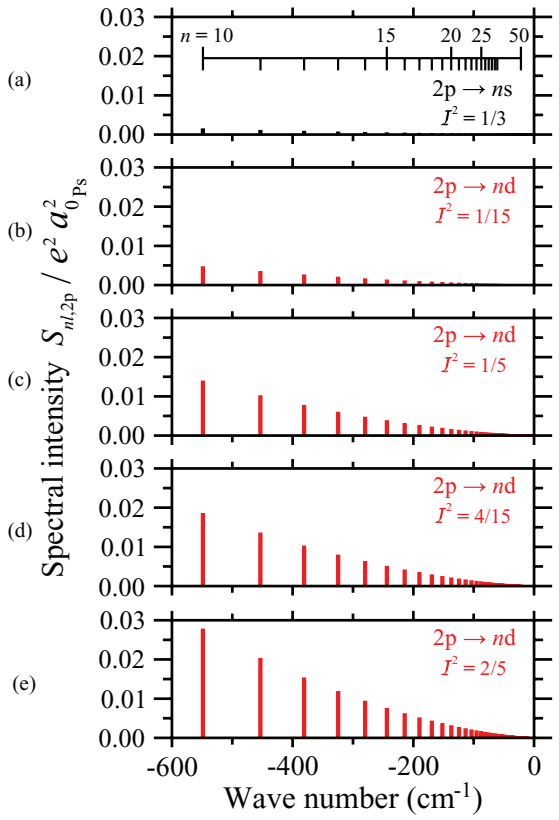

FIG. 2. (Color online) Spectral intensity, $S_{n\ell,2p}$, of electric-dipole transitions from the $2p$ state in Ps to high Rydberg states. (a) Intensity of each of the $\Delta m = 0, \pm 1$ transitions to the ns Rydberg states. (b)–(e) Intensities of each of the dipole-allowed $2p \rightarrow nd$ transitions listed in Table I with the corresponding value of $\mathcal{I}^2$ indicated in each frame.

velocity $\overline{|\vec{v}|} \sim 10^5$ m/s. This results in Doppler widths of the transitions to the Rydberg states on the order of $\sim$10 cm^{-1} (300 GHz) the effect of which can also be seen in Fig. 3(a) (dashed red curve). Because of this Doppler broadening the individual Rydberg states can only be resolved up to $n \simeq 20$.

The fluorescence lifetime of the $10d$ Rydberg state of Ps is 1.08 μs in the absence of external fields while that of the $2p$ state is 3.19 ns. Therefore under continuous illumination, to efficiently transfer population between these two states it is necessary to drive the $2p \rightarrow nd$ transition at Rabi frequencies of $\Omega_{nd,2p} \sim 1$ GHz. Given that

$$\Omega_{nd,2p} = \frac{|\langle nd|\mu|2p\rangle|}{h}\sqrt{\frac{2I_{\text{laser}}}{\epsilon_0 c}}, \tag{2}$$

this requires laser intensities of $I_{\text{laser}} \sim 10^4$ W/cm^2, which can be achieved using nanosecond pulsed lasers. Under these conditions, when the Rabi frequency exceeds the natural linewidth of the transition, saturation occurs and gives rise to a broadening of the corresponding spectral feature. However, this power broadening will only be observable if $\Omega_{nd,2p}$ approaches the spectral linewidth associated with

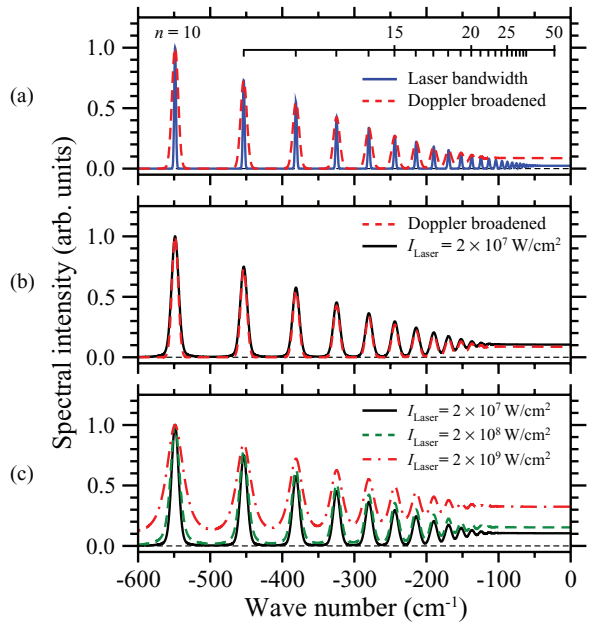

FIG. 3. (Color online) Calculated $2p \rightarrow nd$ photoexcitation spectra of Ps. (a) Laser-bandwidth–limited spectrum (continuous blue curve), and Doppler broadened spectrum (dashed red curve). (b) Doppler broadened spectrum [dashed red curve as in (a)], and Doppler broadened spectrum including power broadening associated with a laser intensity of, $I_{laser} = 2 \times 10^7$ W/cm^2. (c) Doppler broadened spectra including power broadening for the laser intensities indicated. In each panel, the spectra are normalized so that the peak associated with the states for which $n = 10$ has an intensity of 1.

the combined effects of the laser bandwidth and Doppler broadening (∼2.8 cm^{-1} [85 GHz] and ∼10 cm^{-1} [300 GHz], respectively, in the experiments of Cassidy *et al.* [4]).

To achieve a Rabi frequency of ∼50 GHz for the $2p \rightarrow 10d$ transition and thus approach the frequency associated with the laser linewidth, laser intensities of $I_{laser} = 2 \times 10^7$ W/cm^2 are required. The effect of a driving laser field of this intensity on the $2p \rightarrow nd$ photoexcitation spectrum can be seen in Fig. 2(b). Since power broadening is a single atom effect, the resulting spectral line profiles are Lorentzian. In the calculation of these spectra, this Lorentzian contribution to an otherwise Gaussian line profile is included using a Voigt function [30,31]. Comparison of the Doppler broadened spectrum (dashed red curve) with that in which power broadening by the driving laser field is included (solid black curve) reveals only a minor contribution of the effects of power broadening in the wings of the transitions to the states with the lowest values of n. The strong n dependence of the transition moments of electric-dipole transitions to the Rydberg states leads to a significant reduction in Rabi frequency over the range of states included in Fig. 2(b) and a corresponding reduction in the power broadened linewidths.

With higher laser intensities, the effects of power broadening are more clearly visible in the field-free photoexcitation spectra as can be seen in Fig. 2(c). Increasing the laser intensity from $I_{laser} = 2 \times 10^7$ W/cm^2 (solid black curve) to $I_{laser} = 2 \times 10^8$ W/cm^2 (dashed green curve) has the effect that the spectral intensity in the wings of the transitions to the $10d$, $11d$, and $12d$ states becomes more significant. With $I_{laser} = 2 \times 10^9$ W/cm^2 the power broadening reaches the level where the spectral intensity does not return to zero in the wave number ranges between each pair of Rydberg states. However, it is notable, particularly in comparison with the experimentally recorded spectrum reported by Cassidy *et al.* [4], that even under the conditions of significant power broadening when $I_{laser} = 2 \times 10^9$ W/cm^2, the reduction in the magnitude of the spectral intensity maxima associated with each Rydberg state continually decreases as the value of n increases. This observation, together with the dramatic reduction in spectral intensity for values of $n > 18$ in the spectrum of Cassidy *et al.* [4] suggest that external electric or magnetic fields in the photoexcitation volume must contribute and cannot be ignored in the interpretation of the experimental spectrum.

IV. EFFECTS OF EXTERNAL FIELDS

The production of Ps by the collision of positrons with porous silica targets generally requires the presence of a background magnetic field to guide the positrons to the target [3]. The Rydberg photoexcitation spectra of Cassidy *et al.* [4] were recorded in a background magnetic field of 0.16 T, while in the AEgIS experiment a magnetic field of 1.0 T will be present at the position where the ortho-Ps will be photoexcited to Rydberg states [9]. Such background fields can have a significant effect on the Rydberg states. However, Ps is unusual in that the magnetic moments associated with orbital angular momentum of the counter-rotating, oppositely charged electron and positron of equal mass cancel, with the result that the Zeeman effect is dominated by the magnetic moments associated with the spins of the two particles [32–34]. Therefore the strong linear Zeeman energy shifts associated with high values of $|m|$, which can often become significant in high Rydberg states are absent in the Rydberg states of Ps. In the Rydberg states of ortho-Ps in a magnetic field $\vec{B}$, the maximal Zeeman energy splitting resulting from the interaction of the electron and positron magnetic moments with the magnetic field is $2(2\mu_B|\vec{B}|)$, where μ_B is the Bohr magneton. In a field of 0.16 T this leads to a Zeeman splitting of ≃0.3 cm^{-1} (≃9 GHz), which, in the context of the present treatment, is significantly smaller than the spectral resolution associated with the laser bandwidth and Doppler broadening and is therefore neglected. In the larger field of 1.0 T planned in the AEgIS experiment, the corresponding Zeeman splitting will be closer to 1.9 cm^{-1} (55 GHz) and while still smaller than the spectral resolution in Ref. [4] may, for particular orientations of laser polarization, begin to play a more important role if the resolution is enhanced.

In thermal Ps samples for which $\overline{|\vec{v}|} \sim 10^5$ m/s, the dominant effect of a background magnetic field $\vec{B}$ on the Rydberg states is the induced electric field that arises as a result of the motion of the Ps atoms in the magnetic field. This electric field $\vec{F}_{mot} = \vec{v} \times \vec{B}$ gives rise to a motional Stark effect [32–35]. For the fraction of Ps atoms in the experiments

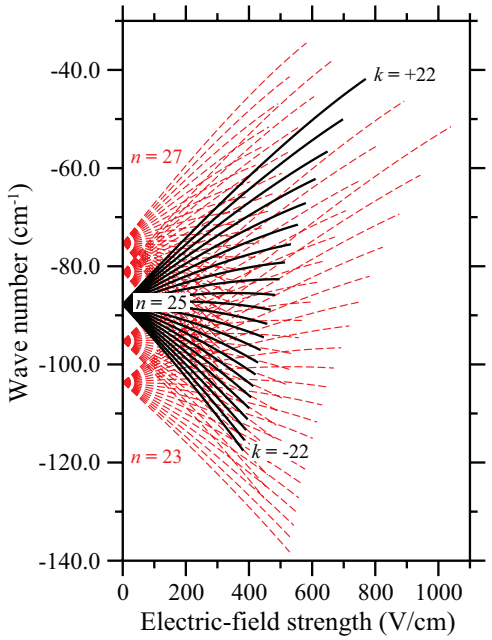

FIG. 4. (Color online) Stark map depicting the energies of the $|m| = 2$ Rydberg states of Ps with values of n between 23 and 27 in the presence of an external electric field. Each state is displayed up to the electric-field strength at which the field-ionization rate exceeds 10^8 s^{-1}.

of Cassidy *et al.* [4] that were moving perpendicular to the background magnetic field of 0.16 T, the resulting motional electric field was $|\vec{F}_{\rm mot}| = 160$ V/cm. In the AE$\bar{\rm g}$IS experiment, Ps atoms moving in a direction perpendicular to the 1 T background magnetic field, with similar translational velocities, would experience a motional electric field of 1000 V/cm.

Rydberg states with high values of n are in general very sensitive to electric fields because of their large electric-dipole moments and linear Stark shifts. The maximum induced electric-dipole moment, $\mu_{\rm elec}$, associated with a Rydberg state of a particular value of n in Ps is

$$\mu_{\rm elec} \simeq \tfrac{3}{2} n^2 \, e \, a_{0_{\rm Ps}} \tag{3}$$

and is 1.999 times greater than that of the corresponding state in the H atom because of the effect of the reduced mass on the magnitude of the Bohr radius. Therefore the Stark energy shifts and the forces that can be exerted on Ps Rydberg atoms by inhomogeneous electric fields are also larger for each value of n than those in the H atom. As demonstrated in the following, the Ps Rydberg photoexcitation spectrum reported in Fig. 4 of Cassidy *et al.* [4] is dominated by effects of external electric fields. These fields are expected to result from a combination of the motional Stark effect, an applied background electric field of 200 V/cm [4], and possible charge buildup on the porous silica target in which the ortho-Ps is produced close to the photoexcitation volume.

The Stark energy shift, $E_{\rm Stark}$, of hydrogenic Rydberg states such as those of Ps, can be calculated analytically in parabolic coordinates using perturbation theory. The result, for an electric field $\vec{F}$, can be expressed to fourth order as [38]

$$\begin{aligned} E_{\rm Stark} = {} & \frac{3}{2} n k \, e \, a_{0_{\rm Ps}} |\vec{F}| \\ & - \frac{1}{16} n^4 (17n^2 - 3k^2 - 9m^2 + 19) \frac{e^2 a_{0_{\rm Ps}}^2}{E_{\rm h}} |\vec{F}|^2 \\ & + \frac{3}{32} n^7 k [23n^2 - k^2 + 11m^2 + 39] \frac{e^3 a_{0_{\rm Ps}}^3}{E_{\rm h}^2} |\vec{F}|^3 \\ & - \frac{1}{1024} n^{10} [5487n^4 + 35182n^2 - 1134m^2 k^2 \\ & + 1806n^2 k^2 - 3402n^2 m^2 + 147k^4 - 549m^4 \\ & + 5754k^2 - 8622m^2 + 16211] \frac{e^4 a_{0_{\rm Ps}}^4}{E_{\rm h}^3} |\vec{F}|^4, \end{aligned} \tag{4}$$

where $E_{\rm h_{Ps}} = 2hc\,{\rm Ry}_{\rm Ps}$ is the Hartree energy for Ps, and k is the difference between the two parabolic quantum numbers n_1 and n_2. For each value of n and $|m|$, k takes values from $-(n - |m| - 1)$ to $+(n - |m| - 1)$ in increments of two. The first term in Eq. (4) represents the linear Stark interaction and is dominant for low values of n and $|m|$ in weak electric fields. In stronger fields the quadratic Stark shift, dependent upon $|\vec{F}|^2$, plays an increasingly important role particularly for higher values of n. This can be seen in Fig. 4, where the energies of the $|m| = 2$ Rydberg states of Ps with values of n between 23 and 27, in electric fields of up to 1000 V/cm are displayed. The curvature of each state toward lower energy with increasing electric field strength is a consequence of the quadratic Stark shift.

Because of their proximity to the ionization limit, high Rydberg states are also susceptible to ionization in the presence of electric fields. The field strength at which ionization begins for each value of n coincides approximately with the classical ionization limit $F_{\rm ion} = E_{\rm h_{Ps}}/(e\,a_{0_{\rm Ps}}\,9n^4)$ [27]. However, within a manifold of Stark states with a particular value of n, the true ionization field strength for each sublevel is dependent upon the value of the index k and the time scale over which ionization can occur. For states with values of $k < 0$, the Rydberg electron charge distribution is localized on the side of the ion core adjacent to the Stark saddle point [36]. As a result, the outermost states on this edge of the Stark manifold ionize in a field approximately equal to that associated with the classical ionization limit. On the other hand, for states with values of $k > 0$, the Rydberg electron charge distribution is localized on the opposite side of the ion core to the Stark saddle point. The Rydberg electron must therefore tunnel around the ion core before ionization occurs and a larger field is required for ionization.

The process of electric field ionization of a Rydberg state can be more precisely described by considering the tunnel ionization rate in the presence of the field $\vec{F}$. Following the treatment of Damburg and Kolosov [37,38], the ionization rate $\Gamma_{n n_1 n_2 m}$ for a Rydberg-Stark state with quantum numbers n, $k = n_1 - n_2$ and m can be

expressed as

$$\Gamma_{n n_1 n_2 m} = \frac{E_{\mathrm{h_{Ps}}}}{\hbar} \frac{(4R)^{2n_2+m+1}}{n^3\, n_2!\,(n_2+m)!} \times \exp\left[-\frac{2}{3}R - \frac{1}{4}n^3 \frac{e\, a_{0_{\mathrm{Ps}}} |\vec{F}|}{E_{\mathrm{h_{Ps}}}} \left(34n_2^2 + 34n_2 m + 46n_2 + 7m^2 + 23m + \frac{53}{3} \right) \right], \quad (5)$$

where

$$R = \frac{1}{e\, a_{0_{\mathrm{Ps}}} \sqrt{E_{\mathrm{h_{Ps}}}}} \frac{(-2E_{n n_1 n_2 m})^{3/2}}{|\vec{F}|} \quad (6)$$

and $E_{n n_1 n_2 m} = -[E_{\mathrm{h_{Ps}}}/(2n^2)] + E_{\mathrm{Stark}}$ is the total energy of the state with respect to the ionization limit, in the presence of the electric field. Under typical experimental conditions where Rydberg photoexcitation and detection take place on nanosecond time scales, ionization rates on the order of 10^8 s^{-1} generally result in complete field ionization of a Rydberg sample. In Fig. 4 the Stark energy shift of each state is displayed up to the electric field strength at which the ionization rate exceeds 10^8 s^{-1}. Under these conditions, it can be seen that for each value of n, the ionization field strength of the outermost state with $k > 0$ is approximately twice as large as that of the outermost state for which $k < 0$.

The spectral intensity of allowed electric-dipole transitions to hydrogenic Rydberg-Stark states such as those of Ps, can be determined by transforming the zero-field parabolic wave functions to a spherical basis. The transformation coefficients, expressed in terms of Wigner-3J symbols, are [27]

$$\langle n n_1 n_2 m | n \ell m \rangle = (-1)^{[(1-n+m+n_1-n_2)/2]+\ell} \times \sqrt{2\ell+1} \begin{pmatrix} \frac{n-1}{2} & \frac{n-1}{2} & \ell \\ \frac{m+n_1-n_2}{2} & \frac{m-n_1+n_2}{2} & -m \end{pmatrix} \quad (7)$$

such that

$$|n n_1 n_2 m\rangle = \sum_{\ell} |n \ell m\rangle \langle n \ell m | n n_1 n_2 m \rangle. \quad (8)$$

By determining the electric-dipole transition strengths to the allowed angular momentum components of each Rydberg-Stark state and associating these with the corresponding eigenenergies given by Eq. (4), a photoexcitation spectrum for transitions from the $2p$, $|m| = 1$ state of Ps to $|m| = 2$ Rydberg states in the presence of an electric field of arbitrary strength can be calculated. Such spectra are depicted in Fig. 5(a) for electric fields of 200 V/cm (upper spectrum) and 500 V/cm (lower spectrum). In these spectra, each transition is indicated by a single vertical line, many of which overlap. The gross spectral behavior is dominated by the n dependence of the transition strength, while for each value of n the intensity distribution associated with the corresponding set of Stark states is governed by Eq. (7).

Inclusion of the effects of a finite laser bandwidth of 85 GHz and the Doppler broadened linewidth of 300 GHz expected for a thermal Ps sample with $\overline{|\vec{v}|} \sim 10^5$ m/s, results in the spectra presented in Fig. 5(b). In this case the gross spectral intensity distribution is again dominated by the decrease in transition strength expected with increasing values of n. In these spectra, the broadening resulting from this combination of laser bandwidth and Doppler linewidth dominate the Stark energy shifts of the states within each Stark manifold for

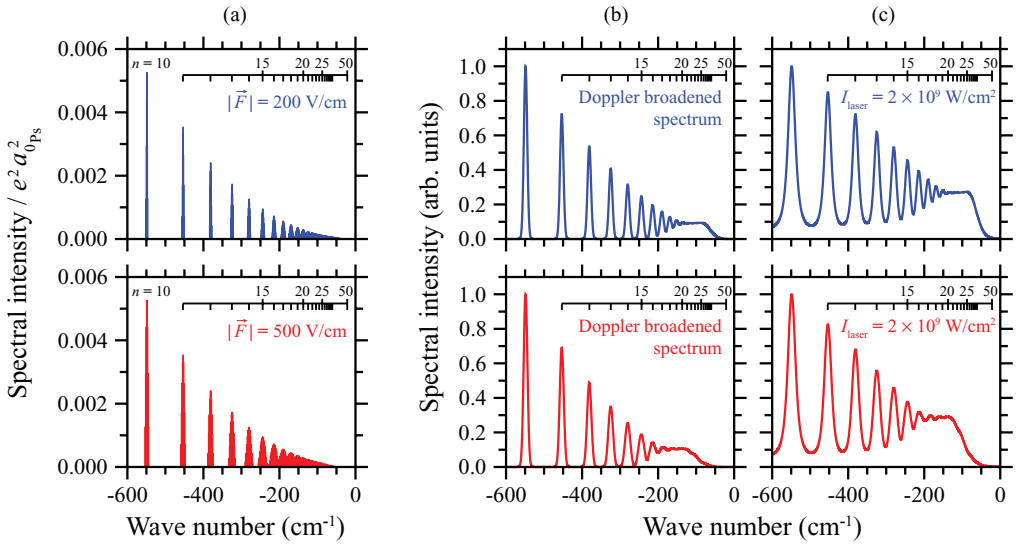

FIG. 5. (Color online) (a) Stick spectrum displaying the spectral intensity of all allowed single-photon electric-dipole transitions from the $2p$, $|m| = 1$ state in Ps to the nd, $|m| = 2$ components of each Rydberg-Stark state in the presence of an electric field of $|\vec{F}| = 200$ V/cm (upper spectrum) and $|\vec{F}| = 500$ V/cm (lower spectrum). (b) as (a) but including the effects of a finite laser bandwidth of 85 GHz and the Doppler broadening expected for a thermal Ps sample with $\overline{|\vec{v}|} \sim 10^5$ m/s. (c) as (b) but including the effects of power broadening resulting from a laser intensity of $I_{\mathrm{laser}} = 2 \times 10^9$ W/cm^2. The spectra in (b) and (c) are normalized so that the peak associated with the states for which $n = 10$ has an intensity of 1.

$n < 15$. However, the effects of the electric field are observable in (i) the difference in spectral overlap between adjacent manifolds of Stark states for values of n between 15 and 20, and (ii) the wave number at which the cutoff in spectral intensity that results from electric field ionization begins. In the field of 200 V/cm (500 V/cm) the last states that can be clearly resolved are those for which $n = 17$ ($n = 19$). While the reduction in spectral intensity resulting from electric field ionization begins at $\simeq -75\ \mathrm{cm}^{-1}$ ($\simeq -125\ \mathrm{cm}^{-1}$) in the field of 200 V/cm (500 V/cm).

If photoexcitation is carried out with a laser intensity of $I_{\mathrm{laser}} = 2 \times 10^9\ \mathrm{W/cm}^2$, power broadening of the transitions in the wave number range in Fig. 5(b) gives rise to the slightly modified spectra depicted in Fig. 5(c). The results of this power broadening are an increase in the spectral width of the transitions associated with each value of n, and an increase in intensity in the wings of each of the main spectral features as a result of the Lorentzian component of the power broadened spectral line shape. The overall effect of power broadening is therefore primarily a reduction in spectral resolution. However, even at this laser intensity of $I_{\mathrm{laser}} = 2 \times 10^9\ \mathrm{W/cm}^2$, the reduction in peak spectral intensity at each of the intensity maxima, with increasing value of n, while not as pronounced as in Fig. 5(b), can still be clearly seen.

For ease of comparison with the experimentally measured spectra reported in Fig. 4 of Cassidy *et al.* [4], the photoexcitation spectrum calculated for an electric field of 500 V/cm in the absence of power broadening [Fig. 5(b), bottom panel] is presented in Fig. 6(a) with the horizontal axis displayed in terms of the wavelength in air of the laser radiation used for photoexcitation. The wavelength range included in this figure is identical to that of Fig. 4 in Ref. [4].

The three most notable features of the data of Cassidy *et al.* [4] are (i) an increase in the spectral width of the transitions as the value of n increases at the longer wavelength end of the spectrum, (ii) a continuous reduction in spectral intensity in the unresolved portion of the spectrum above $n = 18$, and (iii) almost equal peak intensities of the spectral lines, corresponding to transitions to states with values of n between 10 and 14, while between each of these peaks the intensity reduces to the level of the background. Of these points, (i) and (ii) are consistent with the presence of an electric field in the photoexcitation region, with (i) resulting from the increase in the range of electric-dipole moments of the Stark states associated with each value of n, and (ii) an effect of the onset of electric field ionization. Both of these features are also present in the calculated photoexcitation spectrum presented in Fig. 6(a). However, feature (ii) is not present in this calculated spectrum and is therefore not solely a result of the presence of an electric field.

The effects of saturation, within the duration of a coherent Fourier-transform-limited laser pulse, on Rydberg photoabsorption spectra in external electric fields can be seen in Fig. 5(c). Although the n dependence of the peak intensity of each manifold of Stark states is reduced when power broadening becomes significant, this is accompanied by an increase in spectral intensity in the spectral regions between each maximum. The resulting nonzero spectral intensity in the regions between each adjacent pair of states with values of n between 10 and 13 is not observed in the spectrum of

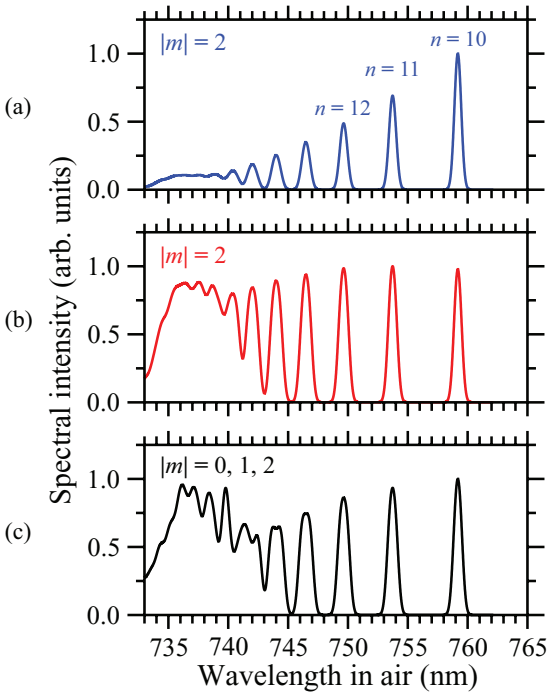

FIG. 6. (Color online) (a) Laser bandwidth and Doppler broadened, $|m| = 2$, Ps Rydberg photoexcitation spectrum in an electric field of 500 V/cm [as Fig. 5(b)] with horizontal axis displayed in terms of the wavelength in air of the laser radiation used for photoexcitation. (b) as (a) but including the effects of saturation in the incoherent radiation field of a multimode laser. (c) as (b) but including all permissible values of $|m|$ of the Rydberg states as would be expected if unpolarized radiation was employed for each step in the two-photon excitation scheme. For ease of comparison each spectrum is normalized in intensity so that the peak associated with the states for which $n = 10$ has an intensity of 1.

Cassidy *et al.* [4]. The indication is therefore that the transitions to the states with these low values of n in the spectrum of Cassidy *et al.* are not saturated by a coherent single-mode radiation field, but rather by an incoherent multimode field. In a coherent radiation field, the oscillatory transfer of population between the two coupled eigenstates states that occurs upon saturation leads to power broadening and Lorentzian line shapes with decreased peak intensity and increased spectral width [see Figs. 3(c) or 5(c)]. However, for particles with high recoil velocities in an incoherent radiation field this oscillatory population transfer does not occur. Under such conditions saturation is instead characterized by a complete transfer of population to the excited state for all transitions with dipole moments greater than a particular value. For a set of transitions to Rydberg states, this gives rise to a series of peak spectral intensities that are, up to certain threshold, almost independent of the value of n as observed by Cassidy *et al.*

Photoabsorption spectra in which these saturation effects are included can be calculated by convoluting the spectral intensity distributions presented in the bottom panel of Fig. 5(a) with Gaussian distribution functions representing the combined laser bandwidth and Doppler broadened spectral profile after having set all transitions with dipole moments larger than a certain threshold value, S_{thres}, to an equal intensity. The spectrum in Fig. 6(b) of the $|m| = 2$ Rydberg states

of Ps in an electric field of 500 V/cm was calculated by setting this threshold transition dipole moment to $S_{\text{thres}} = 0.00045e^2a_0^2$. Under these conditions, this calculated photoabsorption spectrum is in very good qualitative agreement with the experimental spectrum reported by Cassidy *et al.* [4]. This is particularly evident in the n dependence of the widths of the spectral features at wavelengths between 745 nm and 765 nm, and in the approximately linear increase in spectral intensity with wavelength for high values of n, between 733 nm and 736 nm. In the calculated spectrum in Fig. 6(b), the spectral intensity in this wavelength range increases by $\sim$0.25 nm^{-1}, while in the experimental data of Cassidy *et al.* [4] the corresponding change in spectral intensity is $\sim$ 0.2 nm^{-1}. To demonstrate the dependence of the spectral intensity distribution on the value of $|m|$, a spectrum in an equivalent electric field of 500 V/cm in which Rydberg states with all permissible values of $|m|$ are included is presented in Fig. 6(c). This corresponds to the situation that would be expected if unpolarized radiation was employed for each step of a two-photon excitation scheme. In this case $S_{\text{thres}} = 0.00025e^2a_0^2$. The more prominent oscillations in spectral intensity observed in the unresolved part of the spectrum below 740 nm are not consistent with the measurements of Cassidy *et al.* This observation indicates that the spectrum reported by Cassidy *et al.* is predominantly composed of transitions to Rydberg states with $|m| = 2$.

It is important to note that the calculated spectrum in Fig. 6(b) does not include effects of electric field inhomogeneities across the Ps sample at the position of photoexcitation. Such inhomogeneities may be present in experiments of this kind as a feature of the static electric field distribution, or a result of the range of induced motional electric fields experienced by Ps atoms with velocity vectors, which differ in orientation and magnitude. In addition, the precise form of the velocity distribution of the Ps atoms is not treated in the calculations described here. The details of this distribution will have an effect on the Doppler broadened spectral profile and on the magnitude of the induced motional electric fields. To achieve good quantitative agreement between theory and experiment it would also be necessary to consider variations in the mode structure and intensity of the laser radiation employed in the experiment over the wavelength range studied, and possible temporal changes in the electric field distribution resulting from charge buildup.

V. REQUIREMENTS FOR THE PHOTOEXCITATION OF INDIVIDUAL RYDBERG-STARK STATES OF Ps

For the applications of Ps Rydberg atoms described in the Introduction, and for the most efficient implementation of the methods of Rydberg-Stark deceleration of Ps, the preparation of samples in individual Rydberg-Stark states is desirable. This can be achieved with the least stringent requirements on spectral resolution if photoexcitation is carried out in electric fields close to the Inglis-Teller field, F_{IT}. This is the field in which the outermost Stark states at the high-energy edge of one n manifold first cross the outermost Stark states at the low-energy edge of the manifold of states with principal quantum number $n + 1$ [27]. In this field, the energy separation between adjacent Stark states with the same value of n is largest while the states associated with consecutive n manifolds do not spectrally overlap. For Rydberg-Stark states with $m = 0$, the Inglis-Teller field is $F_{\text{IT}_{\text{Ps}}} = E_{\text{h}_{\text{Ps}}}/(e\,a_{0_{\text{Ps}}}3n^5)$. Thus $F_{\text{IT}_{\text{Ps}}} \simeq 565$ V/cm, $\simeq$135 V/cm and $\simeq$45 V/cm, for $n = 15$, 20, and 25, respectively. In these fields the typical energy spacings between the Rydberg-Stark states at each value of n is $\simeq$2.17 cm^{-1} (65.0 GHz), $\simeq$0.69 cm^{-1} (20.7 GHz), and $\simeq$0.29 cm^{-1} (8.7 GHz), respectively. Therefore a spectral resolution of at least 10 GHz will be necessary to resolve individual Rydberg-Stark states with values of n in this range.

In the wave number ranges required to drive the resonant two-photon excitation considered here, single-mode Fourier-transform-limited nanosecond pulsed lasers with bandwidths below 1 GHz would provide the spectral resolution required for the photoexcitation of selected Rydberg-Stark states if a sufficiently homogeneous electric field can be generated across the photoexcitation volume. However, as is the case in the spectrum of Cassidy *et al.* [4], the resolution achievable in these experiments is strongly influenced by motional effects arising directly through Doppler broadening, or indirectly in the broad range of motionally induced electric fields present across the Ps sample. Cancellation of the motional Stark effect can be implemented for selected velocity classes within the Ps sample, as has been achieved in atomic beam experiments [39,40], and the Doppler broadening could be reduced by collimation of the Ps beam. These approaches would however affect the number of ortho-Ps atoms available for photoexcitation. To achieve photoexcitation of the maximal number of atoms within the Ps sample, while ensuring sufficiently high spectral resolution for selective excitation of individual Rydberg-Stark states, nonresonant Doppler-free two-photon excitation directly from the 1s ground state, combined with cancellation of the motional Stark effect using appropriately designed electric field distributions will be required. A Doppler-free Rydberg photoexcitation scheme of this kind has been implemented previously by Lee *et al.* [41] and by Penent *et al.* [42] for rubidium atoms in the presence of combined electric and magnetic fields. For hydrogenic systems the transition dipole moments for these two-photon transitions have been calculated and tabulated by Haas *et al.* [43].

VI. CONCLUSION

The low mass of the Ps atom means that motional effects can play a significant role in the preparation and spectroscopic study of its excited states. These effects can occur directly in the form of Doppler broadening or indirectly as a result of motionally induced electric fields. The results of the calculations presented here have elucidated the origins of the principal features of the experimental Ps Rydberg photoabsorption spectra reported recently by Cassidy *et al.* [4], the role of these motional effects and the effects of saturation of the corresponding electric-dipole transitions. In addition, the main challenges associated with the efficient excitation of Ps Rydberg states in the 1.0 T magnetic fields of the AEgIS antihydrogen experiment have been highlighted. The results presented have also permitted the identification of the prerequisites for the efficient implementation of Rydberg-atom optics elements for Ps, which are expected to play an important role in future precision spectroscopic and gravitational measurements involving these exotic atoms.

APPENDIX

TABLE II. Numerical values of the $|\langle ns|r|2p\rangle|$ and $|\langle nd|r|2p\rangle|$ radial integrals, the squares of which are displayed in Fig. 1, and the spectral intensities, $S_{ns,2p}$ and $S_{nd,2p}$, of each of the transitions presented in Fig. 2.

n	$\lvert\langle ns\rvert r\rvert 2p\rangle\rvert/a_{0_{\mathrm{Ps}}}$	$\lvert\langle nd\rvert r\rvert 2p\rangle\rvert/a_{0_{\mathrm{Ps}}}$	$S_{ns,2p}/e^2a_{0_{\mathrm{Ps}}}^2$ ($\mathcal{I}^2=1/3$)	$S_{nd,2p}/e^2a_{0_{\mathrm{Ps}}}^2$ ($\mathcal{I}^2=1/15$)	$S_{nd,2p}/e^2a_{0_{\mathrm{Ps}}}^2$ ($\mathcal{I}^2=1/5$)	$S_{nd,2p}/e^2a_{0_{\mathrm{Ps}}}^2$ ($\mathcal{I}^2=4/15$)	$S_{nd,2p}/e^2a_{0_{\mathrm{Ps}}}^2$ ($\mathcal{I}^2=2/5$)
10	0.064 7796	0.263 1359	0.001 3988	0.004 6160	0.013 8481	0.018 4641	0.027 6962
11	0.055 4836	0.224 7617	0.001 0261	0.003 3679	0.010 1036	0.013 4714	0.020 2071
12	0.048 2569	0.195 0848	0.000 7762	0.002 5372	0.007 6116	0.010 1488	0.015 2232
13	0.042 4987	0.171 5334	0.000 6020	0.001 9616	0.005 8847	0.007 8463	0.011 7695
14	0.037 8176	0.152 4478	0.000 4767	0.001 5494	0.004 6481	0.006 1974	0.009 2961
15	0.033 9480	0.136 7107	0.000 3842	0.001 2460	0.003 7380	0.004 9840	0.007 4759
16	0.030 7037	0.123 5438	0.000 3142	0.001 0175	0.003 0526	0.004 0702	0.006 1052
17	0.027 9505	0.112 3890	0.000 2604	0.000 8421	0.002 5263	0.003 3683	0.005 0525
18	0.025 5894	0.102 8364	0.000 2183	0.000 7050	0.002 1151	0.002 8201	0.004 2301
19	0.023 5458	0.094 5782	0.000 1848	0.000 5963	0.001 7890	0.002 3853	0.003 5780
20	0.021 7626	0.087 3794	0.000 1579	0.000 5090	0.001 5270	0.002 0360	0.003 0541
21	0.020 1952	0.081 0576	0.000 1359	0.000 4380	0.001 3141	0.001 7521	0.002 6281
22	0.018 8085	0.075 4689	0.000 1179	0.000 3797	0.001 1391	0.001 5188	0.002 2782
23	0.017 5746	0.070 4989	0.000 1030	0.000 3313	0.000 9940	0.001 3254	0.001 9880
24	0.016 4707	0.066 0552	0.000 0904	0.000 2909	0.000 8727	0.001 1635	0.001 7453
25	0.015 4782	0.062 0623	0.000 0799	0.000 2568	0.000 7703	0.001 0271	0.001 5407
26	0.014 5821	0.058 4585	0.000 0709	0.000 2278	0.000 6835	0.000 9113	0.001 3670
27	0.013 7696	0.055 1923	0.000 0632	0.000 2031	0.000 6092	0.000 8123	0.001 2185
28	0.013 0302	0.052 2208	0.000 0566	0.000 1818	0.000 5454	0.000 7272	0.001 0908
29	0.012 3549	0.049 5081	0.000 0509	0.000 1634	0.000 4902	0.000 6536	0.000 9804
30	0.011 7362	0.047 0233	0.000 0459	0.000 1474	0.000 4422	0.000 5897	0.000 8845
31	0.011 1677	0.044 7406	0.000 0416	0.000 1334	0.000 4003	0.000 5338	0.000 8007
32	0.010 6437	0.042 6375	0.000 0378	0.000 1212	0.000 3636	0.000 4848	0.000 7272
33	0.010 1596	0.040 6947	0.000 0344	0.000 1104	0.000 3312	0.000 4416	0.000 6624
34	0.009 7113	0.038 8956	0.000 0314	0.000 1009	0.000 3026	0.000 4034	0.000 6051
35	0.009 2950	0.037 2258	0.000 0288	0.000 0924	0.000 2772	0.000 3695	0.000 5543
36	0.008 9078	0.035 6725	0.000 0264	0.000 0848	0.000 2545	0.000 3393	0.000 5090
37	0.008 5468	0.034 2246	0.000 0243	0.000 0781	0.000 2343	0.000 3124	0.000 4685
38	0.008 2095	0.032 8723	0.000 0225	0.000 0720	0.000 2161	0.000 2882	0.000 4322
39	0.007 8940	0.031 6071	0.000 0208	0.000 0666	0.000 1998	0.000 2664	0.000 3996
40	0.007 5981	0.030 4212	0.000 0192	0.000 0617	0.000 1851	0.000 2468	0.000 3702
41	0.007 3204	0.029 3078	0.000 0179	0.000 0573	0.000 1718	0.000 2291	0.000 3436
42	0.007 0592	0.028 2609	0.000 0166	0.000 0532	0.000 1597	0.000 2130	0.000 3195
43	0.006 8132	0.027 2749	0.000 0155	0.000 0496	0.000 1488	0.000 1984	0.000 2976
44	0.006 5812	0.026 3452	0.000 0144	0.000 0463	0.000 1388	0.000 1851	0.000 2776
45	0.006 3621	0.025 4672	0.000 0135	0.000 0432	0.000 1297	0.000 1730	0.000 2594
46	0.006 1549	0.024 6370	0.000 0126	0.000 0405	0.000 1214	0.000 1619	0.000 2428
47	0.005 9587	0.023 8510	0.000 0118	0.000 0379	0.000 1138	0.000 1517	0.000 2275
48	0.005 7727	0.023 1060	0.000 0111	0.000 0356	0.000 1068	0.000 1424	0.000 2136
49	0.005 5963	0.022 3991	0.000 0104	0.000 0334	0.000 1003	0.000 1338	0.000 2007
50	0.005 4286	0.021 7276	0.000 0098	0.000 0315	0.000 0944	0.000 1259	0.000 1888

[1] C. M. Surko and R. G. Greaves, Phys. Plasmas **11**, 2333 (2004).

[2] D. B. Cassidy, S. H. M. Deng, R. G. Greaves, and A. P. Mills, Rev. Sci. Instrum. **77**, 073106 (2006).

[3] P. Crivelli, U. Gendotti, A. Rubbia, L. Liszkay, P. Perez, and C. Corbel, Phys. Rev. A **81**, 052703 (2010).

[4] D. B. Cassidy, T. H. Hisakado, H. W. K. Tom, and A. P. Mills, Jr., Phys. Rev. Lett. **108**, 043401 (2012).

[5] Antognini *et al.*, Science **339**, 417 (2013).

[6] R. Pohl, R. Gilman, G. A. Miller, and K. Pachucki [Annu. Rev. Nucl. Part. Sci. (to be published)].

[7] B. I. Deutch, M. Charlton, M. H. Holzscheiter, P. Hvelplund, L. V. Jørgensen, H. Knudsen, G. Laricchia, J. P. Merrison, and M. R. Poulsen, Hyperfine Interact. **76**, 151 (1993).

[8] E. A. Hessels, D. M. Homan, and M. J. Cavagnero, Phys. Rev. A **57**, 1668 (1998).
[9] A. Kellerbauer *et al.*, Nucl. Instr. Meth. Phys. Res. B **266**, 351 (2008).
[10] A. P. Mills and M. Leventhal, Nucl. Instr. Meth. Phys. Res. B **192**, 102 (2002).
[11] E. Vliegen and F. Merkt, Phys. Rev. Lett. **97**, 033002 (2006).
[12] E. Vliegen, P. Limacher, and F. Merkt, Eur. Phys. J. D **40**, 73 (2006).
[13] S. D. Hogan and F. Merkt, Phys. Rev. Lett. **100**, 043001 (2008).
[14] Ch. Seiler, S. D. Hogan, H. Schmutz, J. A. Agner, and F. Merkt, Phys. Rev. Lett. **106**, 073003 (2011).
[15] S. D. Hogan, P. Allmendinger, H. Saßmannshausen, H. Schmutz and F. Merkt, Phys. Rev. Lett. **108**, 063008 (2012).
[16] S. Chu and A. P. Mills, Jr., Phys. Rev. Lett. **48**, 1333 (1982).
[17] S. Chu and A. P. Mills, Jr., and J. L. Hall, Phys. Rev. Lett. **52**, 1689 (1984).
[18] M. S. Fee, A. P. Mills, Jr., S. Chu, E. D. Shaw, K. Danzmann, R. J. Chichester, and D. M. Zuckerman, Phys. Rev. Lett. **70**, 1397 (1993).
[19] K. P. Ziock, R. H. Howell, F. Magnotta, R. A. Failor, and K. M. Jones, Phys. Rev. Lett. **64**, 2366 (1990).
[20] R. G. Hulet and D. Kleppner, Phys. Rev. Lett. **51**, 1430 (1983).
[21] D. Delande and J. C. Gay, Europhys. Lett. **5**, 303 (1988).
[22] S. Berko and H. N. Pendleton, Annu. Rev. Nucl. Part. Sci. **30**, 543 (1980).
[23] A. H. Al-Ramadhan and D. W. Gidley, Phys. Rev. Lett. **72**, 1632 (1994).
[24] R. S. Vallery, P. W. Zitzewitz, and D. W. Gidley, Phys. Rev. Lett. **90**, 203402 (2003).
[25] A. I. Alekseev, Sov. Phys. JETP **7**, 826 (1958).
[26] A. I. Alekseev, Sov. Phys. JETP **9**, 1312 (1959).
[27] T. F. Gallagher, *Rydberg Atoms* (Cambridge University Press, Cambridge, 1994).
[28] F. Castelli, I. Boscolo, S. Cialdi, M. G. Giammarchi, and D. Comparat, Phys. Rev. A **78**, 052512 (2008).
[29] H. A. Bethe and E. E. Salpeter, *Quantum Mechanics of One- and Two-Electron Atoms* (Springer, Berlin, 1957).
[30] E. Whiting, J. Quant. Spectrosc. Radiat. Transfer **8**, 1379 (1968).
[31] M. Gharavi and S. G. Buckley, Appl. Spectrosc. **58**, 468 (2004).
[32] H. W. Kendall, Ph.D. thesis, Massachussetts Institute of Technology, 1955.
[33] S. M. Curry, Phys. Rev. A **7**, 447 (1973).
[34] M. L. Lewis and V. W. Hughes, Phys. Rev. A **8**, 625 (1973).
[35] H. Crosswhite, U. Fano, K. T. Lu, and A. R. P. Rau, Phys. Rev. Lett. **42**, 963 (1979).
[36] D. Kleppner, M. G. Littman, and M. L. Zimmerman, in *Rydberg States of Atoms and Molecules*, edited by R. F. Stebbings and F. B. Dunning (Cambridge University Press, Cambridge, 1983).
[37] R. J. Damburg and V. V. Kolosov, J. Phys. B: At. Mol. Phys. **12**, 2637 (1979).
[38] R. J. Damburg and V. V. Kolosov, in *Rydberg States of Atoms and Molecules*, edited by R. F. Stebbings and F. B. Dunning (Cambridge University Press, Cambridge, 1983).
[39] R. J. Elliott, G. Droungas, and J.-P. Connerade, J. Phys. B: At. Mol. Opt. Phys. **28**, L537 (1995).
[40] A. M. Abdulla, S. Hogan, M. S. Zhan, and J.-P. Connerade, J. Phys. B: At. Mol. Opt. Phys. **37**, L147 (2004).
[41] S. A. Lee, J. Helmcke, J. L. Hall, and B. P. Stoicheff, Opt. Lett. **3**, 141 (1978).
[42] F. Penent, D. Delande, and J. C. Gay, Phys. Rev. A **37**, 4707 (1988).
[43] M. Haas, U. D. Jentschura, C. H. Keitel, N. Kolachevsky, M. Herrmann, P. Fendel, M. Fischer, Th. Udem, R. Holzwarth, and T. W. Hänsch, M. O. Scully, and G. S. Agarwal, Phys. Rev. A **73**, 052501 (2006).